Electrochimica Acta 553 (2026) 148285

Contents lists available at ScienceDirect

Electrochimica Acta

journal homepage: www.journals.elsevier.com/electrochimica-acta

Oxygen evolution reaction electrocatalyst based on grafted cobalt and nickel doped carbon dots

Julio Corrales Cristeto [a], Cristina Gutiérrez-Sánchez [a,b,*], Eva Mateo-Martí [c], Encarnación Lorenzo [a,b,d], Emiliano Martínez-Periñán [a,b,*]

[a] Departamento de Química Analítica y Análisis Instrumental, Universidad Autónoma de Madrid, Madrid 28049, Spain
[b] Institute for Advanced Research in Chemical Sciences (IAdChem), Universidad Autónoma de Madrid, Ciudad Universitaria de Cantoblanco, 28049, Madrid, Spain
[c] Centro de Astrobiología (CAB) CSIC-INTA, Ctra. Ajalvir, Km. 4, 28850, Torrejón de Ardoz, Madrid, Spain
[d] IMDEA-Nanociencia, Ciudad Universitaria de Cantoblanco, 28049, Madrid, Spain

ARTICLE INFO

Keywords:
Doped carbon dots
Electrocatalyst
OER
Electrografting

ABSTRACT

Cobalt and nickel co-doped carbon dots (CoNi-CDs) have been synthesized using hydrothermal microwave assisted methodology. CoNi-CDs have been characterized, showing their ability to be diazotized and electrografted onto carbon surfaces, generating an ordered pattern distribution over carbon electrode surfaces. High electrocatalytic activity through oxygen evolution reaction (OER) in basic medium has been proved, showing that the electrocatalyst activity is enhanced when the CoNi-CDs are grafted onto the working electrode instead of just drop-casted. Grafted CoNi-CDs over carbon screen printed electrodes (grafted CoNi-CDs/CSPE) present lower overpotential for OER compared with RuO_2 reference material drop-casted over CSPE. Furthermore, the high turnover frequency of the electrocatalytic centers (cobalt and nickel ions) embedded into the carbon nanostructure enhances the OER electrocatalysis using a small amount of metal for the preparation of the electrocatalyst. In addition, good stability is shown for the modified electrodes used during OER electrocatalyst.

1. Introduction

The development of new electrocatalysts is an interesting field with high economic impact, focusing on the development of clean and renewable energy conversion technologies. The dissociation of water is a pivotal chemical process that facilitates the conversion of fluctuating renewable resources, such as wind and solar power, into storable hydrogen fuel. This mechanism is fundamentally comprised of two distinct half-reactions: the hydrogen evolution reaction (HER) (HER, $2H^+ + 2e^- \rightarrow H_2$) and the oxygen evolution reaction (OER, $2H_2O \rightarrow O_2 + 4H^+ + 4e^-$), being OER the reaction in which the highest overpotentials are required, limiting the applicability of this technology [1]. Great results have been obtained using noble metal-based catalysts such as RuO_2 and IrO_2 as oxygen evolution reaction (OER) electrocatalysts [2]. However, the high cost and low stability under operation conditions have limited their application in real developments. Alternative materials for OER electrocatalysts are being developed, based on nonprecious metals such as metal oxides [3], perovskites [4,5], phosphides [6] and metal hydroxides [7]. These are cheaper alternatives, but in most cases, these materials lack conductivity and require mixing with conductive materials. To address these challenges, various methodologies have been implemented by the scientific community. These include the introduction of foreign ionic species (cations or anions), the induction of structural vacancies, and the optimization of charge transport within electrocatalysts. The latter is often achieved through the integration of highly conductive substrates, such as nickel foam (NF), copper foam (CF) [8], etc.

Owing to their cost-effectiveness, high availability, and superior electrical conductivity, carbon-based nanostructures have emerged as highly efficient materials with extensive surface areas and robust stability [9,10]. Over the last ten years, research into carbon-derived catalysts has surged [11], specifically regarding the enhancement of oxygen reduction reaction (ORR) [12,13] and OER [13,14] performance. Within this category, carbon dots (CDs) stand out due to their unique structural advantages. Unlike other carbon allotropes, the morphology of CDs is characterized by an abundance of active edge sites, which significantly boosts their electrocatalytic efficiency [15], surface modification, good photostability, water dispersibility, low cytotoxicity, and their facile and

* Corresponding authors at: Departamento de Química Analítica y Análisis Instrumental, Universidad Autónoma de Madrid, Madrid 28049, Spain.
E-mail addresses: cristina.gutierrezs@uam.es (C. Gutiérrez-Sánchez), emiliano.martinez@uam.es (E. Martínez-Periñán).

https://doi.org/10.1016/j.electacta.2026.148285
Received 18 November 2025; Received in revised form 15 January 2026; Accepted 20 January 2026
Available online 20 January 2026

cheap synthesis methods [16]. CDs have been synthesized using both the top-down [17] and the bottom-up [18] methods depending upon the required application. Due to the stringent environmental regulations, nowadays, the greenness and sustainability of nanomaterials are major requirements [19]. Using bottom-up strategies, CDs can be synthesized using a great variety of precursors, most of them using natural and abundant compounds like carbohydrates, amino acids, organic acids, etc. Furthermore, their composition can be tailored according to the chemical makeup of the precursors.

Doping strategies have been widely used since the optical, electrical, and catalytic properties of nanomaterials can be modified to the desired extent [20]. The electronic and chemical properties of CDs can be significantly altered through heteroatom doping. This process modifies their nanostructure by facilitating the overlap of atomic orbitals between the dopants and the carbon framework. Furthermore, the inherent electron-donating or withdrawing characteristics of these heteroatoms—known as the push-pull effect—allows for precise tuning of the material's overall composition. Metal ions have also been employed to dope CDs. Metal ions have more electrons and unoccupied orbitals than heteroatoms, and present larger atomic radius. All these are the reasons why doping CDs with metal ions induce important modifications of the electron density distribution and energy gap of the CDs, generating changes in their optical, electronic, and catalytic properties [21]. Furthermore, the introduction of metal centers in the CDs nanostructures allows a good dissemination of the catalytic centers, which results in a high electrocatalytic activity despite the use of low quantities of these metallic centers, optimizing and economizing the production of these electrocatalysts. Among the metal centers that clearly have demonstrated their ability as OER electrocatalysts Fe, Co and Ni should be mentioned [22–28]. In fact, carbon nanodots doped with these metals or a combination of them have already been reported for use as OER electrocatalysts [29]. The role of Co and Ni centers during the OER mechanisms has been previously reported in the literature [30,31].

An important detail of using nanomaterials as electrocatalysts is how they are employed to modify electrodes. They have been widely mixed into catalytic inks that can be employed to modify the working electrode by drop-casting or can be deposited over a very conductive platform based on nickel and/or copper foams. These strategies sometimes lead to the collapse of the nanostructure, generating aggregates whose behavior and properties are different from those reported for the nanomaterial. To address this aspect, new strategies for the modification of electrodes using nanomaterials are being developed. One of these previously reported strategies is the grafting of carbon nanomaterials on carbon surfaces thanks to the generation of diazonium salts in the nanomaterial itself [32,33].

In this work, we have synthesized cobalt and nickel co-doped carbon dots (CoNi-CDs), which present aromatic amines in their structure, allowing the diazonium salt generation and the electrochemical grafting of CoNi-CDs over carbon electrodes. We have shown that the electrocatalytic behavior for OER of the nanomaterial clearly improved when they are grafted onto carbon electrodes compared with just drop-casting strategy. The modified electrodes by electrochemical grafting showed lower overpotential for OER compared with the same carbon electrodes modified with a reference material such as RuO_2. The turnover frequency of the electrocatalyst centers (Cobalt and Nickel ions) embedded in the CDs nanostructure presents a high ratio, proving a great and stable electrocatalyst for OER in basic conditions.

2. Experimental section

2.1. Chemicals

Sigma-Aldrich® provided the L-arginine, 3,3′-diamino-n-methyldipropylamine, and ruthenium (IV) oxide (99.9% trace metals basis), along with the metallic precursors nickel (II) acetate tetrahydrate and cobalt (II) acetate tetrahydrate. Additionally, Potassium hydroxide (90% flakes) and a 5 wt. % Nafion™ perfluorinated resin solution were sourced from the same supplier. Sodium nitrite was acquired from Riedel-de-Haën (Seelze, Germany), while ethanol and 37% HCl were obtained from Merck and Scharlau, respectively.

2.2. Instrumentation

A focused microwave reactor (CEM Discover (Matthews (NC), USA)) was used for cobalt and nickel doped Carbon nanodots (CoNi-CDs) synthesis. The dialysis membrane tubing used had a cutoff value in the 0.1-0.5 kDa range and was obtained from Spectrum Laboratories (Piraeus, Greece).

The Fourier transform infrared (FTIR) spectra of the CoNi-CDs (previously dried), and its precursors were recorded using KBr pressed pellets. The analysis was performed with a Brucker IFS60v spectrometer in the range of 4000 to 500 cm^{-1}.

Lacey carbon support film copper grids (400mesh) from Electron Microscopy Sciences® were employed for transmission electron microscopy (TEM) analyses. Image acquisition was performed using a JEOL 2100 electron microscope.

Zetasizer Nano ZS instrument (Malvern Instrument Ltd.) was used for Zeta potential characterization.

The absorption spectra in the UV-Vis range for the CoNi-CDs and CDs aqueous solutions were acquired using a Shimadzu UV-1900 double beam spectrometer.

Atomic Force Microscopy (AFM) was conducted on a highly ordered pyrolytic carbon (HOPG) surface. Images were recorded with an Agilent 5500 microscope, employing Olympus cantilevers (RC800PSA, 200_20mm) and operating in tapping mode in air.

Surface analysis by X-ray Photoelectron Spectroscopy (XPS) was carried out utilizing a Phoibos 150 MCD system. The spectrometer featured a hemispherical analyzer and an Al Kα monochromatic source (1486.7 eV) with a 7 mm × 20 mm aperture. All measurements were recorded at ambient temperature within an ultra-high vacuum environment (base pressure of 2×10^{-9} mbar). While the broad survey scans were acquired at a pass energy of 30 eV, high-resolution core-level spectra for O (1 s), C (1 s), N (1 s), Co ($2p_{3/2}$) and Ni ($2p_{3/2}$) were collected using a reduced pass energy of 20 eV. The calibration was performed by setting the adventitious carbon C (1s) at 285.0 eV, and the fitting and deconvolution of the XPS spectral regions were carried out using the fitt-xps software.

Electrochemical measurements were performed with a Metrohm-Autolab potentiostat PGSTAT 302 N. Carbon Screen-printed carbon electrodes (CSPE, DRP-110, Metrohm-DropSens) were employed in electrocatalysis experiments. An external homemade saturated calomel electrode (SCE) has been employed as reference in electrochemical measurements. Measurements were carried out in a homemade glass cell using the commercial connector for SPE of Metrohm-DropSens. When HOPG plates were used as electrodes (for surface characterization using AFM), homemade glass and Teflon cell for flat electrodes were employed. In this case a graphite bar was employed as counter electrode, and the same SCE was used as reference electrode.

2.3. Synthesis of Co, Ni doped carbon dots

The synthesis of the CoNi-CDs involved the preparation of a mixture containing 0.5 mmol each of L-arginine and 3,3′-diamino-n-methyldipropylamine, combined with 0.25 mmol of nickel (II) and cobalt (II) acetate tetrahydrates. These precursors were dissolved in 5.5 mol of Milli-Q water within a glass vial. Subsequently, the solution was subjected to thermal treatment using a CEM Discover® microwave system. The process lasted for 180 seconds, steadily achieving 235°C and generating a maximum pressure of 20 bar. The resulting dark-brown solid was recovered and reconstituted in 10 mL of Milli-Q water, followed by filtration through a 0.1 μm pore-size membrane. To ensure high purity, the filtrate underwent a one-week purification process via

dialysis using a 0.5 kDa molecular weight cut-off (MWCO) membrane. CoNi-CDs solution final concentration after purification was 0.74 mg/mL. The amount of cobalt and nickel found in carbon nanodot suspension was determined by atomic absorption spectroscopy, given a concentration of 4.5 mg/L and 7.8 mg/L in the CoNi-CDs suspension respectively. As we have mentioned, CoNi-CDs presents a concentration of 0.74 mg/mL, which corresponds to a percentage of 0.61% and 1.05%. CoNi-CDs suspension was concentrated using low pressure evaporator system, reaching a concentration of 5 mg/mL. The resulting solution was stored at 4°C in the absence of light.

2.4. Electrografting of Co, Ni doped carbon dots over carbon electrodes

The synthesized doped carbon dots were diazotized by mixing 2.5 mg/mL CoNi-CDs in 0.25 M HCl and 1.5×10^{-2} M $NaNO_2$ in an ice bath for different times under study. The electrografting process of the diazotized CoNi-CDs was performed by adding or dipping the reaction mixture on carbon electrodes (CSPE and HOPG, respectively) and cycling the potential between 0.00 and -0.85 V vs. SCE at 0.10 V/s different numbers of scans. Finally, the resulting CoNi-CDs modified electrode (CoNi-CDs /CSPE or CoNi-CDs /HOPG) was washed with purified water.

2.5. Electrochemical measurements for OER electrocatalysis

Once the electrodes are modified by the electrografting of CoNi-CDs, 50 cyclic voltammetry scans between 0.00 and 1.00 V *vs.* SCE at 0.1 V/s are applied in 1 M KOH as a pretreatment for electrode current stabilization.

For OER electrocatalysis analysis, lineal sweep voltammetry (LSV) experiments at 0.01 V/s were applied to the modified electrodes immersed in 1 M KOH. On the fly iR-correction method for cyclic

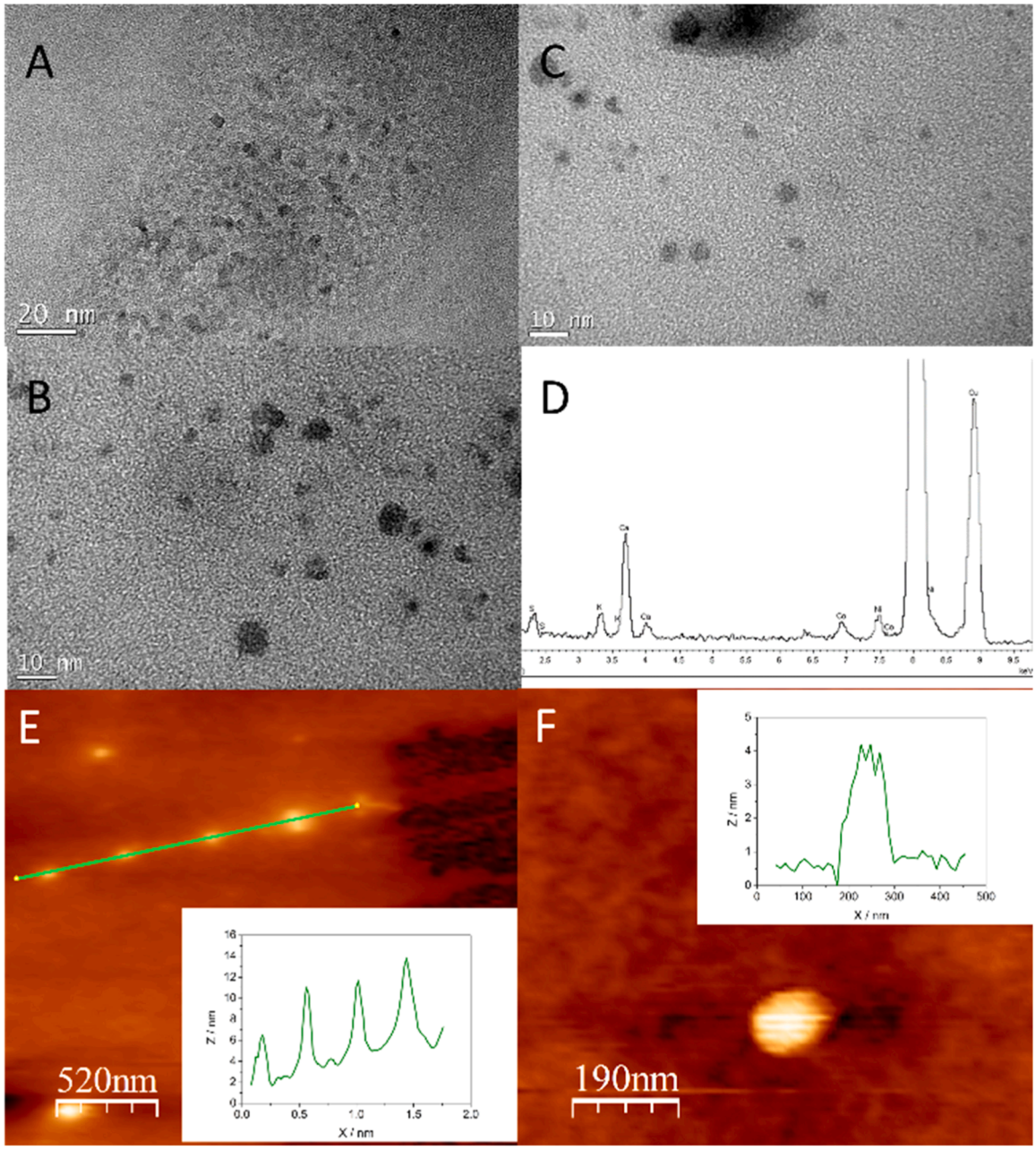

Fig. 1. TEM micrographs of CoNi-CDs at different magnifications 150KX (A), 500KX (B), 500KX (C). EDS spectra of CoNi-CDs (D). AFM topographic image of CoNi-CDs adsorbed on a HOPG surface and topographic profile across the line drawn in green (E,F).

voltammetry (CV) and LSV measurements were used, applying a partial compensation of 85% as it recommended for OER experiments by Jaramillo *et al.* [34].

As reference material for a great OER electrocatalysis, we have employed RuO_2. 1 mg RuO_2/mL suspension was prepared in 20% Ethanol, 0.02 % Nafion water solution. 5 μL of the prepared suspension was dropped-casted over the working electrode of CSPE and then allowed it dry at room temperature.

3. Results and discussion

3.1. CoNi-CDs characterization

CoNi-CDs have been synthesized via hydrothermal synthesis using focused microwave radiation, following a similar procedure as the described by Prato *et al.* [35]. TEM micrographs of synthesized CoNi-CDs can be observed at Fig. 1 (A) (B) and (C) at different magnification grades. CoNi-CDs with quasi-circular shapes are observed, with an average diameter of 3.9 nm. The CoNi-CDs diameter ranges from 2.3 to 5.5 nm. Energy dispersive spectroscopy was used to confirm the presence of Cobalt and Nickel metals in the CoNi-CDs nanostructure. As can be observed at Fig. 1 (D), the peaks corresponding to Cobalt and Nickel are around the main peaks related to the copper of TEM grids employed. Fig. 1 (E and F) shows the AFM topographic images of a HOPG surface after depositing the CoNi-CDs by drop casting. By zooming in one of the CoNi-CDs, individual CoNi-CDs are observed in detail where their circular structure is confirmed. The topographic profiles confirm the result obtained by TEM where the CoNi-CDs have a variable diameter, with an average diameter of 4 nm, agreeing well with TEM results. No aggregates were observed considering both techniques' results.

CoNi-CDs and CDs (absence of Co and Ni) have been characterized by UV-Vis absorption spectroscopy. CDs have been synthesized as a control in the absence of the precursors that contain the metals. In both cases, an absorption band between 250-290 nm is observed, related to π-π* transition of the conjugated C=C and N=C present in the CDs core. This broadband is considerably higher in the case of CoNi-CDs than in the case of CDs, which is evidence of the different effects of nickel and cobalt doping atoms presence in the CoNi-CDs nanostructure.

Further characterization has been carried out using FT-IR spectroscopy (Fig. 2 (B)). In CDs spectrum, the stretching band corresponding to the OH and NH_2 groups was detected as a broad signal with its peak/maximum at 3436 cm^{-1}. In the case of CoNi-CDs a wider band appears, clearly showing a shoulder at 3436 cm^{-1}, and a primary peak at 3252 cm^{-1}. This spectral profile stems from the successful embedding of metal centers within the carbon matrix and the subsequent formation of CoOOH and NiOOH phases. Additionally, the signals identified at approximately 2930 cm^{-1} in both materials are assigned to C-H stretching vibrations, while the C=C vibrational mode at 1647 cm^{-1} in the pure C-dots corroborates the presence of sp^2-hybridized graphitic carbon. This band is wider in the case of CoNi-CDs, covering a range between 1562-1659 cm^{-1}, which agrees with the presence of cobalt and nickel atoms in the carbon dots nanostructure (Co=O and Ni=O vibrations). The band at 1399 cm^{-1} is associated with C-OH, which is ascribed to the presence of more acetate groups (used as metal precursor compounds), being the reason why it increases in the case of CoNi-CDs. The broad band centered at 642 cm^{-1} could be ascribed to Co-O and Ni-O stretching. FT-IR results confirm the presence of both metal ions in the carbon dots nanostructure, showing clear differences with the non-doped CDs.

3.2. Preliminary studies of OER electrocatalysis using CoNi-CDs over carbon electrodes

In order to evaluate the initial catalytic activity of the CoNi-CDs (Fig. 3). In a first approach CoNi-CDs were adsorbed on the surface of the electrode and present a moderate electrocatalytic activity for OER when they are just drop-casted over CSPE (Fig. 3- red line). This initial result aims us to focus our attention on new strategies for immobilization of CoNi-CDs over carbon electrodes that would enhance the electrocatalytic properties. We recently demonstrated that CDs functionalized with aromatic primary amines on their surfaces present very good solubility in aqueous solution and are suitable to be covalently anchored on carbon electrodes by electrografting [36,37].

To verify that the synthesized CDs contain primary aromatic amines, they were electrografted following the protocol described in experimental section. Our first attempt to immobilize CoNi-CDs via

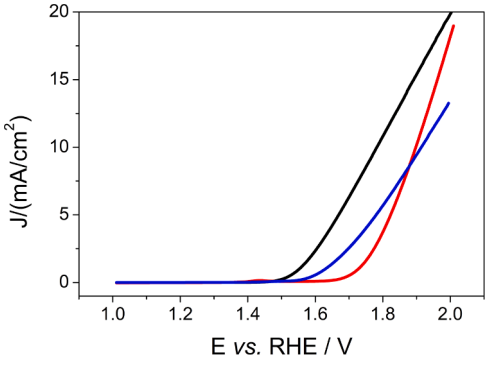

Fig. 3. LSV using RuO_2/CSPE (black), adsorbed-CoNi-CDs/CSPE (red) and grafted-CoNi-CDs/CSPE (blue) in 1 M KOH at 0.01 V/s.

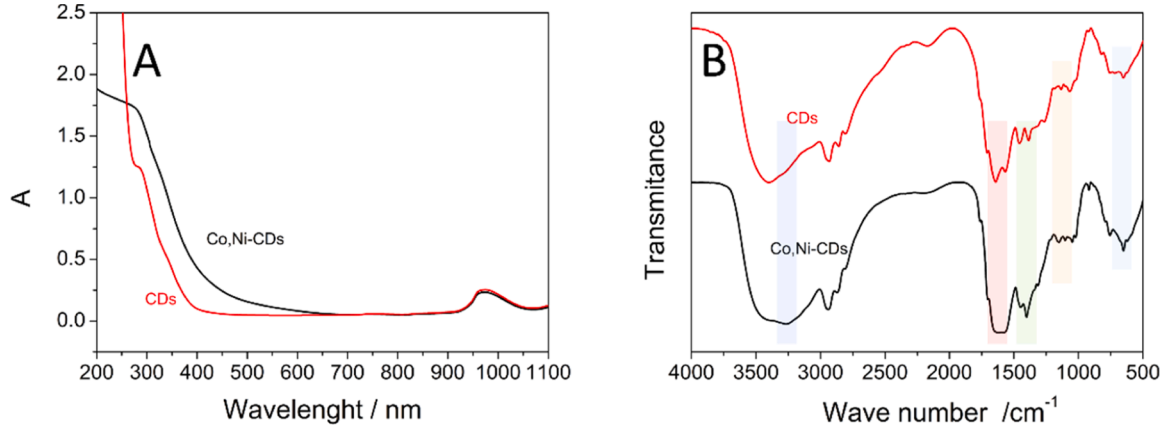

Fig. 2. (A) UV-Vis absorption spectra of CDs (red) and Co,Ni-CDs (black). FTIR spectra of CDs (red) and CoNi-CDs (black).

electrografting showed a good result of the electrocatalytic activity of the modified electrode (Fig. 3-blue line), decreasing the onset potential compared with the drop-cast modified electrode (Fig. 3-black line).

3.3. Electrografting of CoNi-CDs over carbon electrodes

The resulting modified electrodes have been successfully employed for OER electrocatalysis, and regarding the electrocatalytic activity, different aspects of the electrografting process have been optimized. To optimize these parameters, the electrocatalytic activity of electrografted CoNi-CDs/CSPE, modified under different conditions, were analyzed considering the lower onset potential ($J = 10$ mA/cm^2) and determining the overpotential as the difference between the onset potential and the OER standard potential 1.23 V *vs.* RHE.

An important parameter in the electrografting process is to decide the number of cyclic voltammetry scans applied. This parameter has been studied by applying 15, 25, 50 and 100 cyclic voltammetry scans. During these experiments the time required for CoNi-CDs diazotization was fixed at 3 hours. The lower overpotential was determined for 50 scans (Fig. 4 (A)).

We fix 50 scans as the proper electrochemical treatment during electrode modification. Another important aspect is the diazonium salt generation, the time required for the diazotization reaction is a key parameter. We have studied different options, 1, 2, and 3 hours for the reaction time of CoNi-CDs with nitrite in an acidic medium in order to generate the diazonium salt. As can be observed in Fig. 4 (B), the greatest result was obtained using 2 hours as the reaction time for diazotization.

Fig. 5. shows the cyclic voltammetry scans obtained after applying the optimized protocol for electrografting of diazotized CoNi-CDs. As can be observed in the successive scans (Fig. 5. (A)) and clearly in the first scan of the process (Fig. 5. (B)-black line), an irreversible reduction process is observed, decreasing its current intensity in the successive scans. This process at -0.55 V is attributed to the reduction of aryldiazonium groups, generating a highly reactive nucleophilic aryl group that is electrografted on the CSPE. This result confirms that the synthesized CoNi-CDs are rich in aromatic primary amines, allowing direct electrografting onto the electrode surface.

A gradual decrease in the cathodic current associated with this process is observed during successive potential cycles (shown by the red (25th scan) and blue (50th scan) lines in Fig. 5B. This phenomenon is characteristic of electrografting processes. During the successive scans, two reversible redox peaks can be observed at E^0=-0.145 V and E^0=-0.101 V, which are ascribed to hydroxylamine reduction and oxidation of the amine generated. This redox pair appears in the second cycle, that could be due to the reduction of the nitro to amino groups. This reduction is not total, but a portion of hydroxylamine groups remains as such. Control experiments were conducted under identical conditions, utilizing solutions of non-diazotized CoNi-CDs. No reduction process was observed in this scenario (data not presented). These findings validate that the synthesized CoNi-CDs possess surface aromatic amines, which, upon diazotization, facilitate their immobilization via electrografting and the subsequent formation of a covalent bond.

3.4. Modified electrode surface characterization

The carbon surface obtained after modifying it with electrografted CoNi-CDs was studied by AFM and can be seen in Fig. 6. The AFM images in contact mode show that the new surface is covered but not with circular structures associated with individual CoNi-CDs as we saw previously by AFM (Fig. 1 (E,F)) where circular structures randomly distributed throughout the surface, what the AFM image shows is that a new nanopattern has been generated on the surface. The surface coverage is homogeneous, and there is an ordered, quasi-periodic nanopattern of grafted areas associated with the CoNi-CDs and non-grafted areas. We can observe that the nanopattern obtained is due to the grouping of CoNi-CDs and that they are interconnected with each other following a pattern. If we look in more detail at the image that contains the zoom, we can see that individual CDs are distinguished (Fig. 6 (C)). In the topographic profile, it can be seen that the electrografted areas have a height of approximately 1 nm. A height lower than the height found for a CoNi-CDs deposited by drop casting. This fact has been observed previously and could be related to the electrochemical process applied [38]. The formation of these nanopatterns could be due to the formation of stabilized nanobubbles formed within the electrochemical depletion layer, which are assumed to be responsible for protecting the surface of the patterned substrate against grafting by aryl radicals [39].

Successful functionalization by diazotized CoNi-CDs electrografting is confirmed by AFM.

XPS analysis of grafted-CoNi-CDs/CSPE was carried out and compared with drop-casted-CoNi-CDs/CSPE to see the possible composition modifications of CoNi-CDs after the electrografting protocol. As a control, CSPE was also analyzed to see the contribution of CSPE to the XPS analysis of different binding energy regions. Carbon, Nickel, and Cobalt binding energies regions were deeply analyzed (Fig. 7). The carbon 1S region (Fig. 7 (A)) shows, in the case of CSPE, a band deconvolved in three components associated with hydrocarbons (285 eV), C-N bonds (286 eV), and C-O bonds (287 eV). When CSPEs are modified with CoNi-CDs, a significant increment of the components of 286-287 eV occurs, which are associated with Nitrogen and Oxygen functional groups generated over the surface of carbon dots. When CoNi-

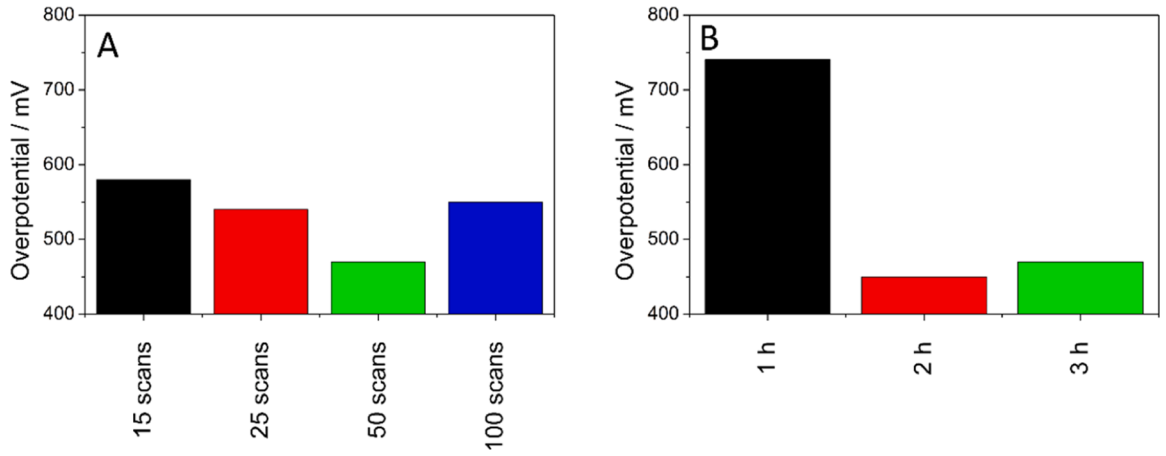

Fig. 4. Onset potential at $J = 10$ mA/cm^2 obtained using grafted CoNi-CDs/CSPE prepared under different conditions: (A) Cyclic voltammetry scans during the electrografting process. (B) CoNi-CDs diazotation reaction time.

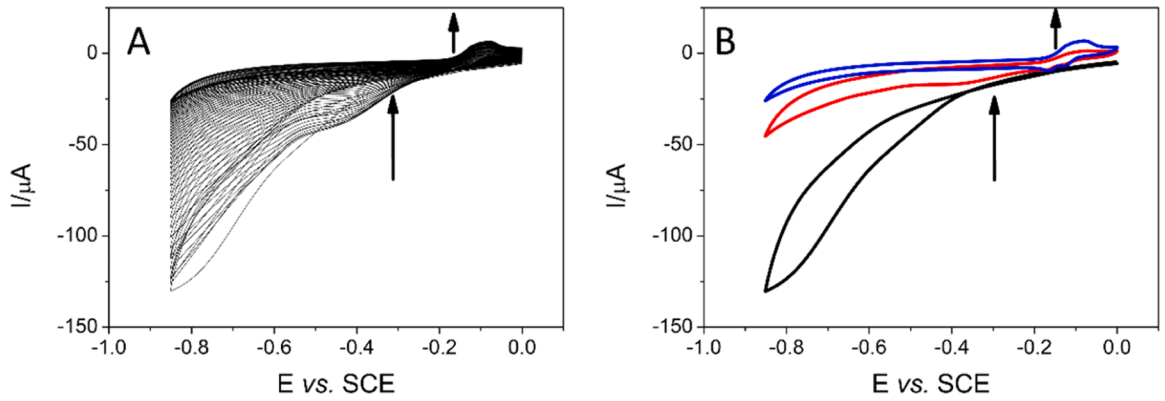

Fig. 5. (A) Successive CV scans (50 scans) of the electrografting process of the CoNi-CDs diazonium salt (2.5 mg/mL) over CSPE in 0.25 M HCl and 1.5 × 10^{-2} M $NaNO_2$ at 0.1 V/s. (B) Selective CV scans from (A): 1st scan (black), 25th scan (red), and 50th scan (blue).

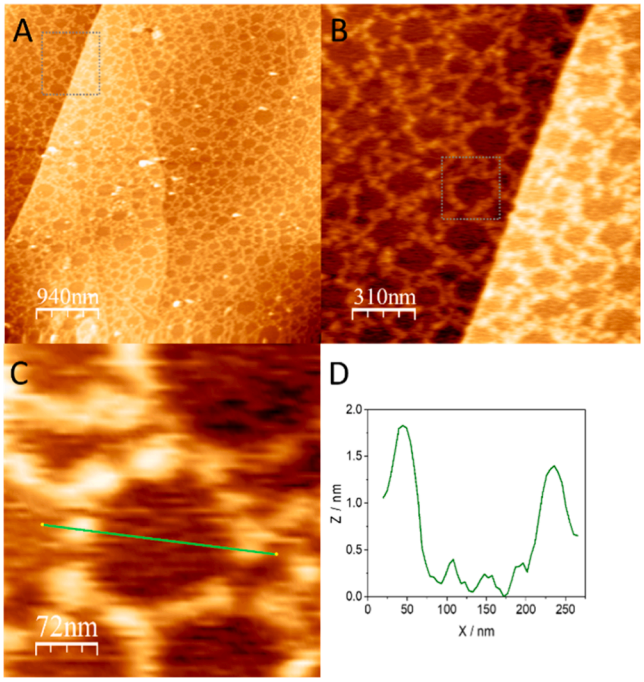

Fig. 6. AFM topographic image of CoNi-CDs electrografting on HOPG surface (A). AFM topography zooms in on the square drawn in Fig. A (B) and in Fig. B (C). Topographic profile across the line drawn in Fig. C (D).

CDs are electrografted with the described protocol, we can observe how the grafting process also modified the carbon 1s region of the surface, decreasing the components 286-287 eV, because of the generation of N_2 during the electrografting process, reducing the amount of nitrogen functional groups over the surface. This result is another evidence of how the electrografting process is working, and it changes the composition of CoNi-CDs. Another significant change observed in the C 1s region is a new component around 292 eV, which has been previously observed in systems associated with π-π* shake-up transitions, which can be associated with the superimposition of carbon nanodots during the grafting process. Furthermore, an intense peak at 294 eV is also observed in the analysis, which corresponds to potassium, doubt to the activation of the grafted-CoNi-CDs/CSPE surface in 1 M KOH (electrocatalysis operation medium), previously to the XPS analysis. The nitrogen region also showed significant information (Fig. 7 (B)). CoNi-CDs drop-cast over CSPE showed a great amount of amine groups, azide, and ammonium groups associated with 400 and 402 eV binding energies, respectively. However, a clear difference in Nitrogen region is observed after electrografting process, in which the amount of nitrogen clearly decreases, as consequence of the production of N_2 during electroreduction process of aryl diazotized amines. Furthermore, a new component at 407.5 eV appears, which is related to nitrates. These ions are generated over the electrode surface as a consequence of the presence of nitrites during the diazotization protocol and the subsequent oxidation of them during the electrochemical activation of the grafted-CoNi-CDs/CSPE surface in 1 M KOH (electrocatalysis operation medium). Regarding nickel region (Fig. 7 (C)), in both drop-cast-CoNi-CDs/CSPE and grafted-CoNi-CDs/CSPE, nickel signal can be observed as it was expected. The detected nickel signal at 856,6 eV binding energy can be associated with nickel acetate environment, which is in good agreement with the nickel precursor employed (nickel (II) acetate tetrahydrate), pointing out that the incorporation of nickel cations into CDs nanostructure are through oxygen coordination. In both cases the same component appears, but a wider band is observed after electrografting process and basic medium activation of grafted-CoNi-CDs/CSPE at 1 M KOH, which can result in new nickel chemical forms such as nickel oxides, nickel hydroxides, etc. Similar results can be deduced from the cobalt binding energies region (Fig. 7 (D)). Cobalt signals can be detected, in less intensity than nickel, in both drop-casted-CoNi-CDs/CSPE and grafted-CoNi-CDs/CSPE, being the binding energies detected of 781 eV. These results confirm even the Cobalt and Nickel atoms incorporation into carbon nanodots structures, as both of them are detected in drop-casted-CoNi-CDs/CSPE, and even that they keep over electrode surface when electrografting process is carried out to attached carbon dots over CSPEs. Furthermore, the changes observed in the carbon region after electrografting process are explained by the electrode surface modification via a grafting process.

3.5. OER electrocatalysis using CoNi-CDs

The platform with the CoNi-CDs/CSPE grafted with the optimized conditions was assessed for its effectiveness as OER electrocatalyst in 1 M KOH (Fig. 8 (A)). Linear scanning voltammetry measurements were performed using the as prepared electrocatalytic platforms. The blue line shows the response offered by grafted-CoNi-CDs/CSPE with the optimized electrografting conditions of the CoNi-CDs, and the response offered can be compared with the electrode used in the presence of RuO_2 (previously drop-casted over CSPE) (black), undoped CDs grafted following the optimized protocol (green), and in a bare CSPE (orange).

As can be seen in Fig. 8 (B) the developed grafted-CoNi-CDs/CSPE clearly decreased the overpotential, not only of a bare CSPE, but even of a CSPE modified with undoped CDs grafted following the optimized protocol and with a CSPE modified with a reference electrocatalyst as RuO_2, decreasing the overpotential around 160 mV. Tafel slopes have been also analyzed (Fig. 8 (C)), showing that in the case of grafted-CoNi-CDs/CSPE a value of 83.5 mV/dec which is lower than the Tafel slope

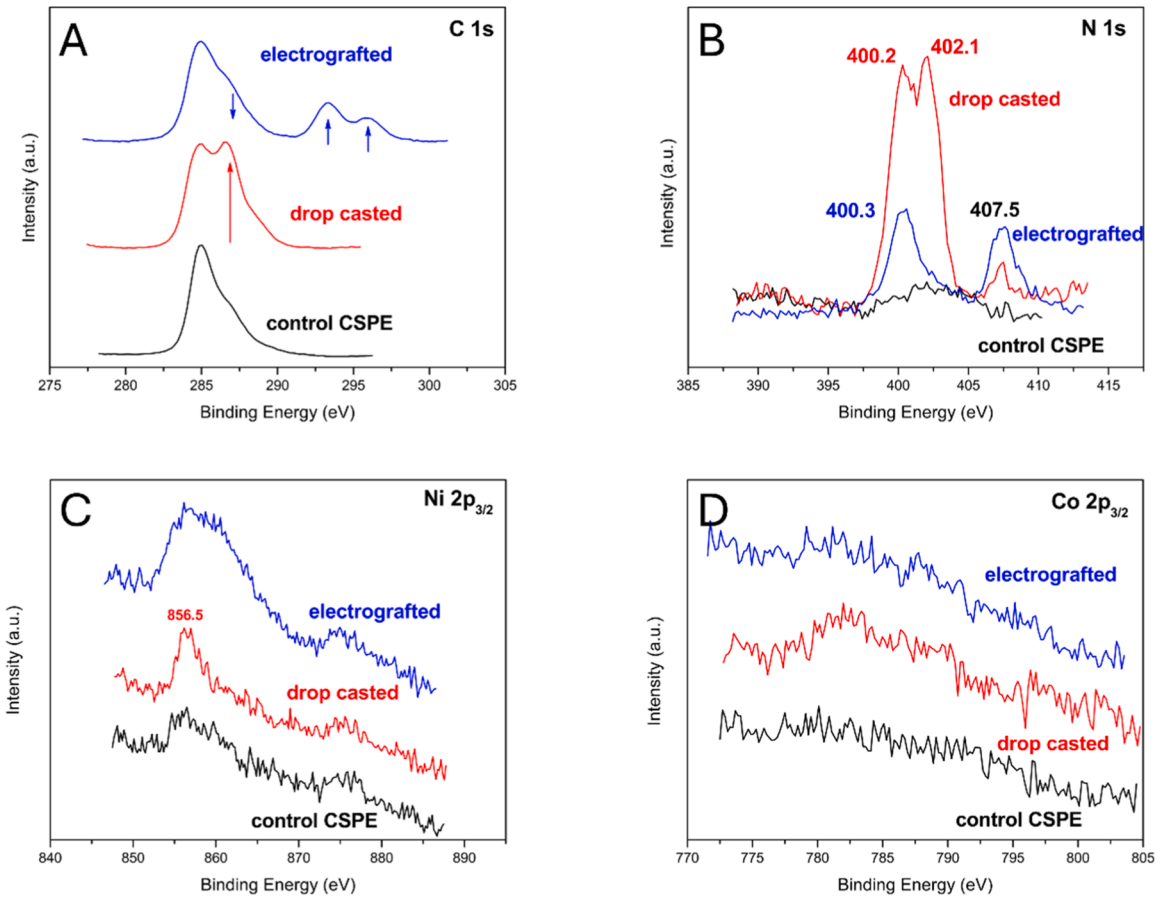

Fig. 7. XPS analysis of CSPE (black), drop-casted-CoNi-CDs/CSPE (red) and grafted-CoNi-CDs/CSPE (blue) at different binding energies regions: C 1s (A), N 1s (B), Ni $2p_{3/2}$(C) and Co $2p_{3/2}$ (D).

determined for the reference material RuO_2/CSPE (95.7 mV/dec). Turn Over Frequency (TOF) of the electrocatalyst was calculated considering that only the metal atoms (nickel and cobalt) are the responsible of electrocatalyzed the OER. The amount of cobalt and nickel moles over the modified electrode were obtained from the charge of the cyclic voltammetry peak related with the oxidation processes $Ni(OH)_2 \leftrightarrow$ NiOOH and $Co(OH)_2 \leftrightarrow$CoOOH (Fig. S1) applying equation (1):

$$n = Q / (Fx\nu)$$

where n is the number of moles electrochemical active, F is the Faraday constant and ν is the number of electron exchange during the redox process (ν=1). From this data we consider that the amount of cobalt and nickel atoms are $4.4{\cdot}10^{-9}$ moles. To calculate the TOF equation (2) was employed:

$$TOF = I / (4{\cdot}F{\cdot}n)$$

Where I is the current intensity of OER electrocatalytic process at 1.675 V *vs.* RHE (1.26 mA), F is the Faraday constant, and n is the number of moles of electrocatalyst involved in the OER ($4.4{\cdot}10^{-9}$ moles).

The TOF obtained from the previous equation gives us a result of 0.74 s^{-1}. This extraordinary result is the consequence of the great accessibility of hydroxyl ions to the metal centers dispersed over the CoNi-CDs nanostructure, obtaining great electrocatalytic behavior with a small amount of metal centers presence over the modified electrode.

The electrochemical double-layer capacitance (Cdl) of CoNi-CDs/CSPE grafted was calculated to estimate the electrochemically active surface area (ECSA) obtaining a capacitance value of 28.3 μF and a ECSA of 0.708 cm^2 Figure S2. For comparison with other reported electrocatalysts current density of LSV obtained from CoNi-CDs/CSPE grafted has been included in figure S3. As can be observed, the grafting protocol enhances in factor of 6 the geometric area of the employed electrodes, helping also with the electrocatalytic process.

Nanomaterials composed of nanoclusters with various metals are described in the literature as acting as excellent electrocatalysts for oxidation and evolution reactions [40–42]. Because they offer metal centers capable of improving the conductivity as well as the kinetics of the catalysts based on their Tafel slopes for the OER [43]. Based on this, a mechanism for OER on electrodes has been proposed based on charge transfer at a surface-active site of a metal [44,45]. The incorporation of Cobalt and Nickel sites, present as either nanoparticles or surface-anchored species, facilitates multi-electron transfer by lowering activation energies. This is achieved through the effective adsorption and stabilization of critical intermediates, specifically *OH, *O, and *OOH. Concurrently, nitrogen doping within the carbon lattice alters the electronic environment, redistributing electron density around the metal centers to further anchor reaction intermediates. The resulting synergy between the metallic sites and the N-doped framework minimizes overpotentials and accelerates reaction kinetics. Throughout the Oxygen Evolution Reaction (OER), the metal sites undergo a cycle from M-OH to M-O and M-OOH, eventually evolving O_2 and regenerating the active site. This interplay optimizes adsorption energies and ensures rapid charge-transfer pathways, leading to superior electrocatalytic activity [46–48].

Electrocatalyst stability is a key factor required in the development of energy devices. We have analyzed the stability of grafted-CoNi-CDs/CSPE applying successive LSV. Fig. 8 (D) showed how the electrochemical activity almost does not decrease during this long experiment, showing just a decrease of 20% of their initial current density at E =

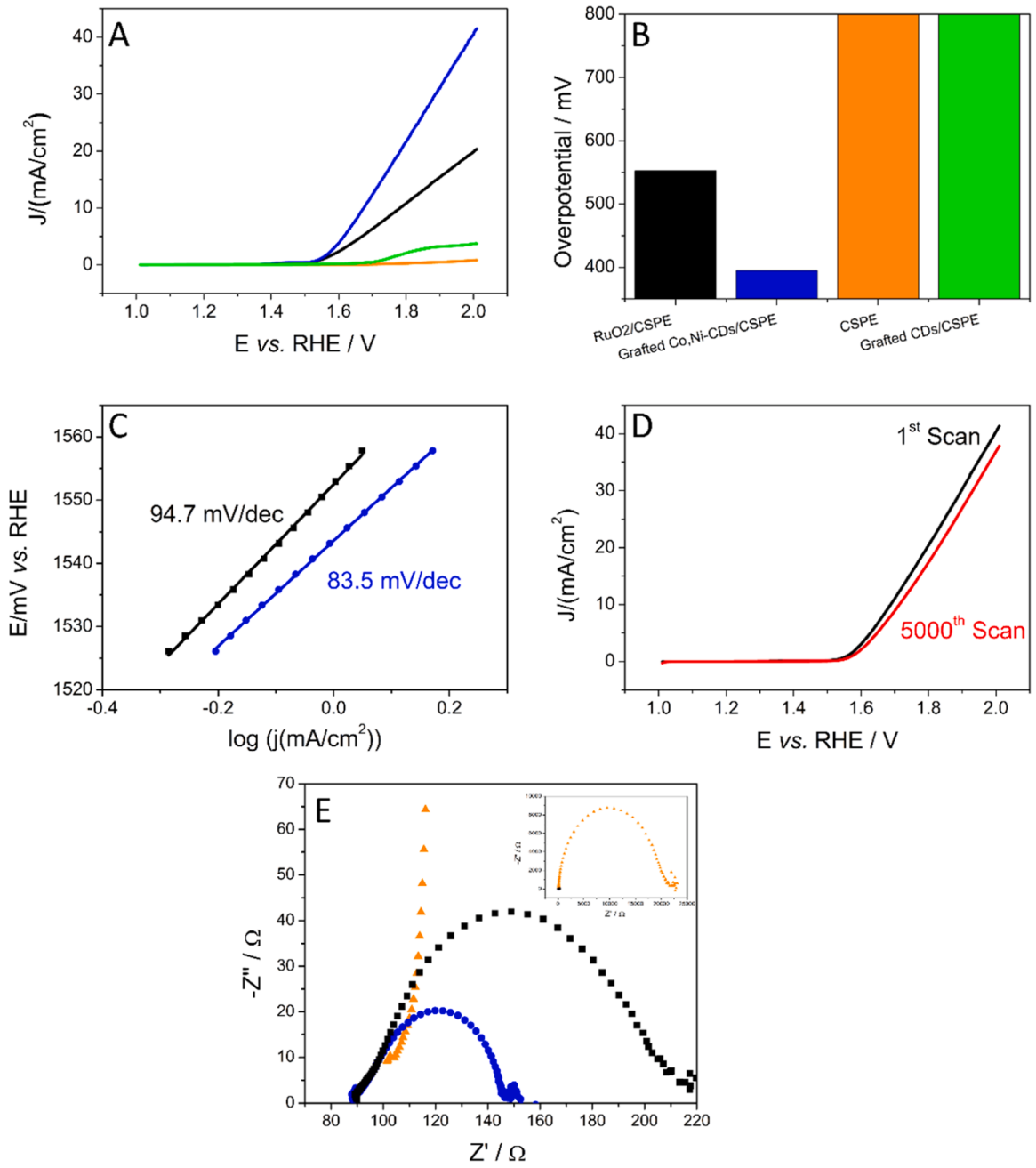

Fig. 8. (A) LSV using RuO_2/CSPE (black), grafted-CoNi-CDs/CSPE (blue), grafted-CDs/CSPE (green) and CSPE (orange) in 1 M KOH at 0.01 V/s. (B) Onset potential at J = 10 mA/cm^2 obtained from (A). (C) Tafel slope obtained from (A). (D) Successive LSV using grafted-CoNi-CDs/CSPE: 1st scan (black) and 5000th scan (red) in 1 M KOH at 0.01 V/s. (E) Nyquist Plot obtained from EIS experiments using RuO_2/CSPE (black), grafted-CoNi-CDs/CSPE (blue) and CSPE (orange) in 1 M KOH at E = 1.675 V vs. RHE.

1.625 V *vs.* RHE (onset potential j = 10 mA/cm^2).

EIS experiments were carried out to study the interfacial properties of the developed surfaces. As can be observed at Fig. 8 (E) the smallest charge transfer resistance is obtained using the developed electrode grafted-CoNi-CDs/CSPE, being lower than electrode modified with a reference material as OER electrocatalyst (RuO_2/CSPE). Which suggests that grafted-CoNi-CDs/CSPE is much more conductive. As we expected, the difference is huge between the unmodified CSPE and the grafted-CoNi-CDs/CSPE.

The state of the art of new OER electrocatalysts based on carbon nanodots can be analyzed in Table 1. Unless great electrocatalyst with lower overpotential have been previously developed, our methodology allows a competitive electrocatalyst with great and competitive TOF value, which makes them affordable and very sustainable as small number of metals atoms are required for its development. Remarking our developed electrocatalysts platform (CoNi-CDs/CSPE), we can mention a very competitive TOF with other reported electrocatalysts, and good result regarding the overpotential at 10 mA/cm^2, which results in a competitive overpotential value unless lower values have been demonstrated. A key point of the developed electrocatalyst platform is the use of economic carbon screen printed electrodes, instead of using Ni foam. The developed methodology can be used in other carbonaceous materials, opening new possibilities for the modification of highly porous carbon materials, which can enhance the OER electrolytic activity.

Table 1
OER electrocatalysts based on carbon nanodots.

Electrocatalyst	Electrolyte	Electrode	Overpotential (mV) @ 10 mA/cm^2	Tafel slope (mV/dec)	TOF (s^{-1})	Ref.
$NiCo_2S_4$ flower N,S doped carbon dots	0.1 M KOH	GCE/RDE	390	85.6	5	[49]
$NiCo/NiCo_2S_4$ N and S co-doped carbon nanofibers	1 M KOH	GC	370	60	-	[50]
N-doped CDs with W doped CoP	1 M KOH	Ni foam	305	118.6	-	[51]
Oxygen plasma-treated graphene QDs embedded Ni-Fe Prussian blue analogue	1 M KOH	Ni foam	259	52.5	0.001	[52]
Carbon Quantum Dots-Doped $Ni_3Se_4/Co_9Se_8/Fe_3O_4$ Multilayer Nanosheets	1 M KOH	GC	268	64	-	[53]
Ni, Fe bimetallic sulfide nanocages with anchored N-doped CDs	0.1 M KOH	GC	295	78.01	0.722	[54]
Cobalt ferrite/graphitic carbon nitride/N doped graphene QDs	1 M KOH	GC	445	69	81	[55]
Nitrogen-doped CDs modified $FeCoS_y$ nanosheets	1 M KOH	GC	284	52.1	0.099	[56]
Nitrogen-doped CDs on nanostructure of CoMoP	1 M KOH	Ni foam	370	67	-	[57]
CDs into cobalt-based zeolitic imidazolate framework in the presence of carbon cloth	1 M KOH	Carbon cloth	256	147	-	[58]
Co,Ni-CDs grafted over CSPE	1 M KOH	CSPE	395	83.5	0.74	This work

4. Conclusions

In summary, we have designed and synthesized Cobalt and Nickel doped carbon nanodots (CoNi-CDs) using a facile microwave-based synthesis method with controlled temperature and pressure. The catalyst showed improved and robust activity for the oxygen evolution reaction (OER) in alkaline medium and presents a lower overpotential for OER compared to the reference material RuO_2. The embedding of a small number of metals ions inside the carbon nanodot, confirmed by XPS, has been sufficient to obtain a high turnover frequency. The electrocatalytic performance of CoNi-CDs reached a promising current density of 40 mA/cm^2 and remarkable robust stability for the OER in alkaline media. The high performance obtained has been due to the electrografting of the CoNi-CDs on a carbon surface, that has resulted in surface modification with an ordered nanopattern and a uniform distribution of the CoNi-CDs, as confirmed by AFM. We believe that the findings obtained in this work will not only provide a guide for the design of more efficient and stable catalysts but also open a new path for further exploration of the structure of electrocatalysts by expanding knowledge in catalytic mechanisms and DFT calculations.

Funding sources

This work has been supported by the Comunidad Autónoma de Madrid (2021-5A/BIO-20943 and SI3/PJI/2021-00341) and the Spanish Ministerio de Ciencia e Innovación (PID2020-116728RB-I00, TED2021-129738B-I00, RED2022-134120-T and PID2022-142262OA-I00).

CRediT authorship contribution statement

Julio Corrales Cristeto: Investigation. **Cristina Gutiérrez-Sánchez:** Writing – original draft, Funding acquisition, Conceptualization. **Eva Mateo-Martí:** Formal analysis, Data curation. **Encarnación Lorenzo:** Supervision, Funding acquisition, Conceptualization. **Emiliano Martínez-Periñán:** Writing – review & editing, Writing – original draft, Funding acquisition, Conceptualization.

Declaration of competing interest

The authors declare that they have no known competing financial interests or personal relationships that could have appeared to influence the work reported in this paper.

Acknowledgements

We would like to thank Santos Gálvez-Martínez for his help with XPS measurements.

Supplementary materials

Supplementary material associated with this article can be found, in the online version, at doi:10.1016/j.electacta.2026.148285.

Data availability

The data supporting this article have been included in https://doi.org/10.21950/ST9MRP.

References

[1] N.-T. Suen, S.-F. Hung, Q. Quan, N. Zhang, Y.-J. Xu, H.M. Chen, Electrocatalysis for the oxygen evolution reaction: recent development and future perspectives, Chem. Soc. Rev. 46 (2017) 337–365, https://doi.org/10.1039/C6CS00328A.
[2] S. Park, Y. Shao, J. Liu, Y. Wang, Oxygen electrocatalysts for water electrolyzers and reversible fuel cells: status and perspective, Energy Environ. Sci. 5 (2012) 9331–9344, https://doi.org/10.1039/C2EE22554A.
[3] F. Song, L. Bai, A. Moysiadou, S. Lee, C. Hu, L. Liardet, X. Hu, Transition metal oxides as electrocatalysts for the oxygen evolution reaction in alkaline solutions: An application-inspired renaissance, J. Am. Chem. Soc. 140 (2018) 7748–7759, https://doi.org/10.1021/jacs.8b04546.
[4] R.A. Rincón, E. Ventosa, F. Tietz, J. Masa, S. Seisel, V. Kuznetsov, W. Schuhmann, Evaluation of perovskites as electrocatalysts for the oxygen evolution reaction, Chemphyschem 15 (2014) 2810–2816, https://doi.org/10.1002/cphc.201402137.
[5] Y. Sun, R. Li, X. Chen, J. Wu, Y. Xie, X. Wang, K. Ma, L. Wang, Z. Zhang, Q. Liao, Z. Kang, Y. Zhang, A-site management prompts the dynamic reconstructed active phase of perovskite oxide OER catalysts, Adv. Energy Mater. 11 (2021) 2003755, https://doi.org/10.1002/aenm.202003755.
[6] W. Li, D. Xiong, X. Gao, L. Liu, The oxygen evolution reaction enabled by transition metal phosphide and chalcogenide pre-catalysts with dynamic changes, Chem. Commun. 55 (2019) 8744–8763, https://doi.org/10.1039/C9CC02845E.
[7] F. Chen, W. Zhou, L. Jia, X. Liu, T. Sasaki, R. Ma, Transition-metal hydroxide nanosheets with peculiar double-layer structures as efficient electrocatalysts, Chem. Catal. 2 (2022) 867–882, https://doi.org/10.1016/j.checat.2022.02.015.
[8] H. Jung, A. Karmakar, A. Adhikari, R. Patel, S. Kundu, Graphene-based materials as electrocatalysts for the oxygen evolution reaction: a review, Sustain. Energy Fuels 6 (2022) 640–663, https://doi.org/10.1039/D1SE01716K.
[9] M. Musameh, N.S. Lawrence, J. Wang, Electrochemical activation of carbon nanotubes, Electrochem. Commun. 7 (2005) 14–18, https://doi.org/10.1016/j.elecom.2004.10.007.
[10] R. Liu, D. Wu, X. Feng, K. Müllen, Nitrogen-doped ordered mesoporous graphitic arrays with high electrocatalytic activity for oxygen reduction, Angew. Chem. Int. Ed. 49 (2010) 2565–2569, https://doi.org/10.1002/anie.200907289.
[11] I.K. Sideri, N. Tagmatarchis, Noble-metal-free doped carbon nanomaterial electrocatalysts, Chem. – Eur. J. 26 (2020) 15397–15415, https://doi.org/10.1002/chem.202003613.
[12] Z. Yang, H. Nie, X. Chen, X. Chen, S. Huang, Recent progress in doped carbon nanomaterials as effective cathode catalysts for fuel cell oxygen reduction reaction, J. Power. Sources 236 (2013) 238–249, https://doi.org/10.1016/j.jpowsour.2013.02.057.
[13] Z. Zhao, M. Li, L. Zhang, L. Dai, Z. Xia, Design principles for heteroatom-doped carbon nanomaterials as highly efficient catalysts for fuel cells and metal–air batteries, Adv. Mater. 27 (2015) 6834–6840, https://doi.org/10.1002/adma.201503211.

[14] Y. Zhao, R. Nakamura, K. Kamiya, S. Nakanishi, K. Hashimoto, Nitrogen-doped carbon nanomaterials as non-metal electrocatalysts for water oxidation, Nat. Commun. 4 (2013) 2390, https://doi.org/10.1038/ncomms3390.
[15] T. Xing, Y. Zheng, L.H. Li, B.C.C. Cowie, D. Gunzelmann, S.Z. Qiao, S. Huang, Y. Chen, Observation of active sites for oxygen reduction reaction on nitrogen-doped multilayer graphene, ACS Nano 8 (2014) 6856–6862, https://doi.org/10.1021/nn501506p.
[16] H. Li, Z. Kang, Y. Liu, S.-T. Lee, Carbon nanodots: synthesis, properties and applications, J. Mater. Chem. 22 (2012) 24230–24253, https://doi.org/10.1039/C2JM34690G.
[17] D. Nagarajan, D. Gangadharan, S. Venkatanarasimhan, Chapter 1 - Synthetic strategies toward developing carbon dots via top-down approach, in: S.K. Kailasa, C.M. Hussain (Eds.), Carbon Dots in Analytical Chemistry, Elsevier, 2023, pp. 1–13, https://doi.org/10.1016/B978-0-323-98350-1.00016-5.
[18] P.D. Modi, V.N. Mehta, V.S. Prajapati, S. Patel, J.V Rohit, Chapter 2 - Bottom-up approaches for the preparation of carbon dots, in: S.K. Kailasa, C.M. Hussain (Eds.), Carbon Dots in Analytical Chemistry, Elsevier, 2023, pp. 15–29, https://doi.org/10.1016/B978-0-323-98350-1.00022-0.
[19] H.B.D. Saruchi, Kumar Vaneet, Green and sustainable future with consumer nanoproducts, in: handbook of consumer nanoproducts, Kumar, Springer Nature Singapore, Singapore, 2022, pp. 1455–1471, https://doi.org/10.1007/978-981-16-8698-6_84.
[20] Y.-P. Sun, X. Wang, F. Lu, L. Cao, M.J. Meziani, P.G. Luo, L. Gu, L.M. Veca, Doped carbon nanoparticles as a new platform for highly photoluminescent dots, J. Phys. Chem. C 112 (2008) 18295–18298, https://doi.org/10.1021/jp8076485.
[21] X. Li, Y. Fu, S. Zhao, J. Xiao, M. Lan, B. Wang, K. Zhang, X. Song, L. Zeng, Metal ions-doped carbon dots: Synthesis, properties, and applications, Chem. Eng. J. 430 (2022) 133101, https://doi.org/10.1016/j.cej.2021.133101.
[22] H.Y. Jung, J.H. Park, J.C. Ro, S.J. Suh, Fabrication of trimetallic Fe–Co–Ni electrocatalysts for highly efficient oxygen evolution reaction, ACS. Omega 7 (2022) 45636–45641, https://doi.org/10.1021/acsomega.2c06461.
[23] L. Li, X. Cao, J. Huo, J. Qu, W. Chen, C. Liu, Y. Zhao, H. Liu, G. Wang, High valence metals engineering strategies of Fe/Co/Ni-based catalysts for boosted OER electrocatalysis, J. Energy Chem. 76 (2023) 195–213, https://doi.org/10.1016/j.jechem.2022.09.022.
[24] M. Yang, T. Feng, Y. Chen, X. Zhao, B. Yang, Ionic-state cobalt and iron co-doped carbon dots with superior electrocatalytic activity for the oxygen evolution reaction, ChemElectroChem 6 (2019) 2088–2094, https://doi.org/10.1002/celc.201900423.
[25] A. Moysiadou, S. Lee, C.-S. Hsu, H.M. Chen, X. Hu, Mechanism of oxygen evolution catalyzed by cobalt oxyhydroxide: cobalt superoxide species as a key intermediate and dioxygen release as a rate-determining step, J. Am. Chem. Soc. 142 (2020) 11901–11914, https://doi.org/10.1021/jacs.0c04867.
[26] N. Hales, T.J. Schmidt, E. Fabbri, Reversible and irreversible transformations of Ni-based electrocatalysts during the oxygen evolution reaction, Curr. Opin. Electrochem. 38 (2023) 101231, https://doi.org/10.1016/j.coelec.2023.101231.
[27] G.-P. Wu, Y.-Y. Wang, D.-H. Li, C.-X. Lu, W.-Z. Shen, X.-T. Li, Z.-H. Feng, Direct electrochemical attachment of carbon nanotubes to carbon fiber surfaces, Carbon. N. Y. 49 (2011) 2152–2155, https://doi.org/10.1016/j.carbon.2011.01.026.
[28] C. Gutiérrez-Sánchez, M. Mediavilla, T. Guerrero-Esteban, M. Revenga-Parra, F. Pariente, E. Lorenzo, Direct covalent immobilization of new nitrogen-doped carbon nanodots by electrografting for sensing applications, Carbon. N. Y. 159 (2020) 303–310, https://doi.org/10.1016/j.carbon.2019.12.053.
[29] F. Arcudi, L. Đorđević, M. Prato, Synthesis, Separation, and characterization of small and highly fluorescent nitrogen-doped carbon nanoDots, Angew. Chem. Int. Ed. 55 (2016) 2107–2112, https://doi.org/10.1002/anie.201510158.
[30] T. Guerrero-Esteban, C. Gutiérrez-Sánchez, E. Martínez-Periñán, M. Revenga-Parra, F. Pariente, E. Lorenzo, Sensitive glyphosate electrochemiluminescence immunosensor based on electrografted carbon nanodots, Sens. Actuators. B Chem. 330 (2021) 129389, https://doi.org/10.1016/j.snb.2020.129389.
[31] T. Guerrero-Esteban, C. Gutiérrez-Sánchez, A.M. Villa-Manso, M. Revenga-Parra, F. Pariente, E. Lorenzo, Sensitive SARS-CoV-2 detection in wastewaters using a carbon nanodot-amplified electrochemiluminescence immunosensor, Talanta 247 (2022) 123543, https://doi.org/10.1016/j.talanta.2022.123543.
[32] C. Gutiérrez-Sánchez, E. Martínez-Periñán, E. Mateo-Martí, E. Lorenzo, In situ" hexagonal nanostructures surface growth from boron-carbon nanodots, Surf. Interfaces 64 (2025) 106425, https://doi.org/10.1016/j.surfin.2025.106425.
[33] T.H. Phan, H. Van Gorp, Z. Li, T.M. Trung Huynh, Y. Fujita, L. Verstraete, S. Eyley, W. Thielemans, H. Uji-i, B.E. Hirsch, S.F.L. Mertens, J. Greenwood, O. Ivasenko, S. De Feyter, Graphite and graphene fairy circles: A bottom-up approach for the formation of nanocorrals, ACS Nano 13 (2019) 5559–5571, https://doi.org/10.1021/acsnano.9b00439.
[34] J. Del Pilar Albadalejo, S. Alonso-Sevilla, N.I. Cintrón, X. Feng, Á.D. García, D. D. Martínez-Torres, A.M. Rodríguez, N.I. Román-Montalvo, J.I. Torres, Y. Yang, A. Peña-Duarte, R. Singhal, L.M. Debefve, C.J. Pollock, C.R. Cabrera, H.D. Abruña, M.B. Santiago-Berríos, Ex Situ and in situ analyses of the mechanism of electrocatalytic hydrogen peroxide production by CoxZn1–xO ($0 < x < 0.018$) materials in alkaline media, ACS. Appl. Energy Mater. 5 (2022) 6597–6605, https://doi.org/10.1021/acsaem.1c04030.
[35] A.L. Maulana, P.-C. Chen, Z. Shi, Y. Yang, C. Lizandara-Pueyo, F. Seeler, H. D. Abruña, D. Muller, K. Schierle-Arndt, P. Yang, Understanding the structural evolution of IrFeCoNiCu high-entropy alloy nanoparticles under the acidic oxygen evolution reaction, Nano Lett. 23 (2023) 6637–6644, https://doi.org/10.1021/acs.nanolett.3c01831.
[36] H. Wang, H.D. Abruña, Designing synergistic electrocatalysts for H2 oxidation and evolution reactions in alkaline media, J. Phys. Chem. C 125 (2021) 7188–7203, https://doi.org/10.1021/acs.jpcc.1c00126.
[37] J. Park, Y.J. Sa, H. Baik, T. Kwon, S.H. Joo, K. Lee, Iridium-Based Multimetallic Nanoframe@Nanoframe structure: an efficient and robust electrocatalyst toward oxygen evolution reaction, ACS Nano 11 (2017) 5500–5509, https://doi.org/10.1021/acsnano.7b00233.
[38] J. Zhang, G. Chen, D. Sun, Y. Tang, W. Xing, H. Sun, X. Feng, Regulating Co–O covalency to manipulate mechanistic transformation for enhancing activity/durability in acidic water oxidation, Chem. Sci. 15 (2024) 17900–17911, https://doi.org/10.1039/D4SC05547K.
[39] E. Antolini, Iridium as catalyst and cocatalyst for oxygen evolution/reduction in acidic polymer electrolyte membrane electrolyzers and fuel cells, ACS Catal. 4 (2014) 1426–1440, https://doi.org/10.1021/cs4011875.
[40] M.S. Amjadi, H. Ashassi-Sorkhabi, M.G. Hosseini, B.G. Pollet, E. Asghari, N/S-RCQD@NiCo2S4 nanocomposite with wrinkled nanosheet-like edges as an anode for water splitting, J. Energy Storage 72 (2023) 108364, https://doi.org/10.1016/j.est.2023.108364.
[41] H. Yu, D. Zhang, Z. Fang, S. Xu, Q. Liu, H. Hou, L. Wang, Z. Zhou, G. Shao, W. Yang, J. Teng, S. Chen, N and S Co-doped carbon nanofibers with embedded candle soot and designed surface decoration for efficient bifunctional electrocatalysts, Electrochim. Acta 380 (2021) 138261, https://doi.org/10.1016/j.electacta.2021.138261.
[42] M. Sun, Q. Zhang, M. Geng, Y. Cui, Q. Lu, L. Wang, L. Du, G. Yin, Carbon dots-coupled with urchin-like tungsten-doped CoP as efficient bifunctional electrocatalysts for overall water splitting, J. Cryst. Growth 624 (2023) 127430, https://doi.org/10.1016/j.jcrysgro.2023.127430.
[43] Y.-C. Lin, S. Aulia, M.-H. Yeh, L.-Y. Hsiao, A.M. Tarigan, K.-C. Ho, Graphene quantum dots induced defect-rich NiFe Prussian blue analogue as an efficient electrocatalyst for oxygen evolution reaction, J. Colloid. Interface Sci. 648 (2023) 193–202, https://doi.org/10.1016/j.jcis.2023.05.187.
[44] Y. Zhang, R. Wang, L. Zhu, X. Li, C. Sun, H. Liu, L. Zhu, K. Wang, Carbon quantum dots-doped Ni3Se4/Co9Se8/Fe3O4 multilayer nanosheets prepared using the One-step solvothermal method to boost electrocatalytic oxygen evolution, Materials 16 (2023), https://doi.org/10.3390/ma16145115.
[45] R. Wang, J. Liu, J. Xie, Z. Cai, Y. Yu, Z. Zhang, X. Meng, C. Wang, X. Xu, J. Zou, Hollow nanocage with skeleton Ni-Fe sulfides modified by N-doped carbon quantum dots for enhancing mass transfer for oxygen electrocatalysis in zinc-air battery, Appl. Catal. B 324 (2023) 122230, https://doi.org/10.1016/j.apcatb.2022.122230.
[46] B.S. Reghunath, S. Rajasekaran, S. Devi K R, D. Pinheiro, J.R. Jaleel UC, N-doped graphene quantum dots incorporated cobalt ferrite/graphitic carbon nitride ternary composite for electrochemical overall water splitting, Int J Hydrog. Energy 48 (2023) 2906–2919, https://doi.org/10.1016/j.ijhydene.2022.10.169.
[47] L. Wu, H. Qin, Z. Ji, H. Zhou, X. Shen, G. Zhu, A. Yuan, Nitrogen-doped carbon dots modified Fe–Co sulfide nanosheets as high-efficiency electrocatalysts toward oxygen evolution reaction, Small. n/a (n.d.) 2305965. 10.1002/smll.202305965.
[48] J. Han, J. Wu, S. Guan, R. Xu, J. Zhang, J. Wang, T. Guan, Z. Liu, K. Li, Interference effect of nitrogen-doped CQDs on tailoring nanostructure of CoMoP for improving high-effective water splitting, Electrochim. Acta 438 (2023) 141595, https://doi.org/10.1016/j.electacta.2022.141595.
[49] Q. Hong, Y. Wang, R. Wang, Z. Chen, H. Yang, K. Yu, Y. Liu, H. Huang, Z. Kang, P. W. Menezes, In situ coupling of carbon dots with Co-ZIF nanoarrays enabling highly efficient oxygen evolution electrocatalysis, Small 19 (2023) 2206723, https://doi.org/10.1002/smll.202206723.
[50] H. Yu, D. Zhang, Z. Fang, S. Xu, Q. Liu, H. Hou, L. Wang, Z. Zhou, G. Shao, W. Yang, J. Teng, S. Chen, N and S Co-doped carbon nanofibers with embedded candle soot and designed surface decoration for efficient bifunctional electrocatalysts, Electrochim. Acta 380 (2021) 138261. doi:10.1016/j.electacta.2021.138261.
[51] M. Sun, Q. Zhang, M. Geng, Y. Cui, Q. Lu, L. Wang, L. Du, G. Yin, Carbon dots-coupled with urchin-like tungsten-doped CoP as efficient bifunctional electrocatalysts for overall water splitting, J. Cryst. Growth 624 (2023) 127430, https://doi.org/10.1016/j.jcrysgro.2023.127430.
[52] Y.-C. Lin, S. Aulia, M.-H. Yeh, L.-Y. Hsiao, A.M. Tarigan, K.-C. Ho, Graphene quantum dots induced defect-rich NiFe Prussian blue analogue as an efficient electrocatalyst for oxygen evolution reaction, J. Colloid Interface Sci. 648 (2023) 193–202, https://doi.org/10.1016/j.jcis.2023.05.187.
[53] Y. Zhang, R. Wang, L. Zhu, X. Li, C. Sun, H. Liu, L. Zhu, K. Wang, Carbon quantum dots-Doped Ni3Se4/Co9Se8/Fe3O4 multilayer nanosheets prepared using the One-Step solvothermal method to boost electrocatalytic oxygen evolution, Materials 16 (2023), https://doi.org/10.3390/ma16145115.
[54] R. Wang, J. Liu, J. Xie, Z. Cai, Y. Yu, Z. Zhang, X. Meng, C. Wang, X. Xu, J. Zou, Hollow nanocage with skeleton Ni-Fe sulfides modified by N-doped carbon quantum dots for enhancing mass transfer for oxygen electrocatalysis in zinc-air battery, Appl. Catal. B 324 (2023) 122230, https://doi.org/10.1016/j.apcatb.2022.122230.
[55] B.S. Reghunath, S. Rajasekaran, S. Devi K R, D. Pinheiro, J.R. Jaleel UC, N-doped graphene quantum dots incorporated cobalt ferrite/graphitic carbon nitride ternary composite for electrochemical overall water splitting, Int. J. Hydrogen Energy 48 (2023) 2906–2919. doi:10.1016/j.ijhydene.2022.10.169.
[56] L. Wu, H. Qin, Z. Ji, H. Zhou, X. Shen, G. Zhu, A. Yuan, Nitrogen-doped carbon dots modified Fe–Co Sulfide nanosheets as high-efficiency electrocatalysts toward

oxygen evolution reaction, Small n/a (n.d.) 2305965, doi:10.1002/smll.202305965.

[57] J. Han, J. Wu, S. Guan, R. Xu, J. Zhang, J. Wang, T. Guan, Z. Liu, K. Li, Interference effect of nitrogen-doped CQDs on tailoring nanostructure of CoMoP for improving high-effective water splitting, Electrochim. Acta 438 (2023) 141595, https://doi.org/10.1016/j.electacta.2022.141595.

[58] Q. Hong, Y. Wang, R. Wang, Z. Chen, H. Yang, K. Yu, Y. Liu, H. Huang, Z. Kang, P. W. Menezes, In situ coupling of carbon dots with Co-ZIF nanoarrays enabling highly efficient oxygen evolution electrocatalysis, Small 19 (2023) 2206723, https://doi.org/10.1002/smll.202206723.